

Ring-based ML calibration with *in situ* pileup correction for real-time jet triggers

Benjamin T. Carlson^{1,2,*} Stephen T. Roche^{3,2,†} Michael Hemmett¹ and Tae Min Hong^{2,‡}

¹*Department of Physics and Engineering, Westmont College, Santa Barbara CA, 93108*

²*Department of Physics and Astronomy, University of Pittsburgh, Pittsburgh PA, 15260*

³*School of Medicine, Saint Louis University, St. Louis MO, 63103*

(Dated: July 23, 2025)

We present a machine learning (ML) method to calibrate hadronic jet energy in real-time trigger systems of the High-Luminosity Large Hadron Collider (HL-LHC) using an efficient implementation on field programmable gate arrays (FPGA). Regression is done to estimate the transverse energy of jet candidates, using concentric rings of electromagnetic and hadronic contributions in 0.1×0.1 towers around fixed-radius cone jet seeds, that accounts for *in situ* pileup correction. Classification separates hard-scatter jets from those due to pileup using the same inputs; its output provides a correction for the regression estimate. The algorithm is tested on simulated samples using an ATLAS-inspired detector in the dense environment of 200 simultaneous proton-proton collisions per bunch crossing. Our method improves the signal efficiency of saving Higgs pair production in $HH \rightarrow b\bar{b}b\bar{b}$ by a factor of two over the traditional cone jet algorithm in real-time trigger systems.

Introduction.—Precise determination of hadronic jet energy is essential for the flagship physics goals at CERN’s High-Luminosity Large Hadron Collider (HL-LHC) [1], one of which is the study of the Higgs potential with hadronic final states [2–7]. Improved calibration in the real-time trigger system that decides whether to keep or discard the events would lower the trigger threshold. This, in turn, increases the yield of events that contain Higgs boson pairs that decay to b -quarks, *i.e.*, $HH \rightarrow b\bar{b}b\bar{b}$ (HH_{4b}), which improves the experimental sensitivity to the Higgs potential through self-coupling [8–11].

Calibration of jet energy from a quark or gluon that emerges from the hadronization process is challenging in the dense environment of the $\langle \mu \rangle = 200$ simultaneous proton-proton collisions per bunch crossing at the HL-LHC. The current state-of-the-art algorithm used in the software trigger and offline reconstruction is to run a sequence beginning with particle flow that connects the tracker and calorimeter systems [12–14], followed by constituent subtraction that are used as input to jet finding using the anti- k_t algorithm [15–21]. The jet objects are corrected by average pileup in proportion to the jet area [22, 23]. Finally, calibration and pileup rejection taggers are performed on the jet candidates [24–29].

The above sequence is the standard algorithm for offline data analyses, but the experiments at the HL-LHC do not have sufficient computing resources at the real-time trigger systems, which need efficient implementations that can be evaluated in fixed latency of $\mathcal{O}(1) \mu\text{s}$ [30–34]. In particular, the underlying anti- k_t algorithm may add challenges in implementing on field programmable gate arrays (FPGA) due to its iterative

design. Typically, simpler fixed-radius cone-based algorithms have been used in real-time systems [35, 36]. Alternative approaches [37, 38] build on advances in machine learning (ML) for FPGA, including neural networks [39, 40] and boosted decision trees (BDT) [41–44]. Our approach is to take cone jets as inputs to perform FPGA-optimized classification and regression.

Setup.—We created simulated samples using publicly available Monte Carlo software. Two samples were made

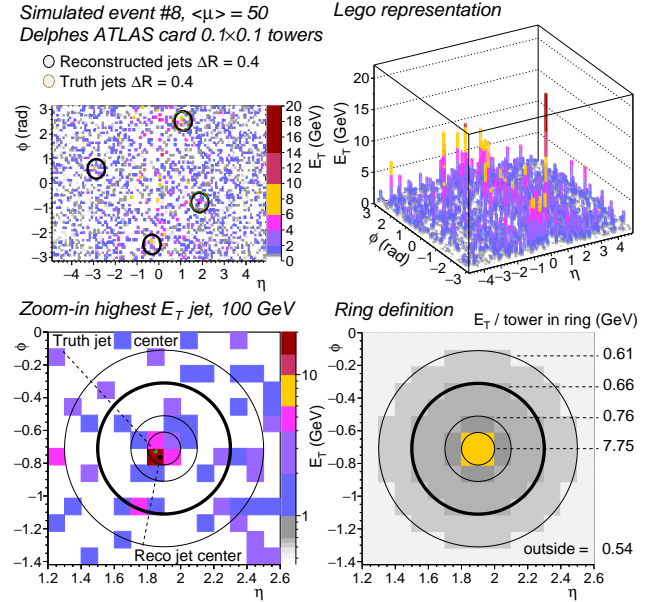


FIG. 1. Simulated dijet event. Top row: Tower E_T with 4 truth jets (circles) and 2 of them matching anti- k_t jets with $\eta > 0$. $E_T^{\text{jet}} > 20$ GeV is applied. Bottom row: 100 GeV jet, its E_T^{tower} (left), and ring₁₋₄ definition and $\langle E_T^{\text{tower}} \rangle_{\text{ring}}$ (right). The region *outside* is for the 0.7×0.7 square outside ring₄.

* bcarlson@westmont.edu

† stephen.roche@health.slu.edu

‡ tmhong@pitt.edu

[45], each with 100k pp collision events: dijet events for the primary background and HH_{4b} for the signal. Simultaneous pp collisions were simulated by overlaying each event with a number of pileup events generated separately with $\langle\mu\rangle=200$ [46], corresponding to the expected levels at Run 4 and 5 of HL-LHC (2030-2041) [47, 48]. (Samples of $\langle\mu\rangle=50$ were also made to cross check.) The physics processes were generated with MadGraph5 3.5.0 [49]. The generation of pileup events, showering, and hadronization were done by Pythia8 [50]. Detector simulation and event reconstruction were performed by Delphes 3.4 using the ATLAS card with pileup [51]. One example dijet event at $\langle\mu\rangle=50$ is shown on the top row of Fig. 1; two generator-level “truth jets” and four anti- k_t reconstructed jets are identified; the bottom row zooms-in on the 100 GeV jet with rings defined later.

Electromagnetic (EM) and hadronic (HAD) calorimeter energies are used as inputs to estimate the jet energy projected to the plane transverse to the beam direction (E_T). The η - ϕ resolution of the inputs is 0.1×0.1 , like the ATLAS Trigger Towers in Run 2 (2015–2018) [52] and jFEX Towers in Run 3 (2022–2026) [53]. The sample of reconstructed jets are identified with the anti- k_t clustering algorithm with a minimum $E_T > 20$ GeV and a radius parameter $R=0.4$ with FastJet [54] using the particle flow (PFlow) energy reconstruction algorithm with pileup (PU) suppression. In this paper, these are referred to as “offline jets” as they are similar to jets in the software-based algorithms for offline processing as well as for the High Level Trigger systems [12].

Our approach is to consider a jet candidate after they are created at the real-time trigger system and apply our ML on it to calibrate the jet E_T . To mock-up a realistic scenario, we deploy a sliding window algorithm on calorimeter towers, inspired by ATLAS [36], to create a set of “primitive jets” [55]. If a primitive jet is within $\Delta R < 0.3$ of any offline jet, where $(\Delta R)^2 = (\Delta\eta)^2 + (\Delta\phi)^2$, it is considered “matched” to a “HS jet” from the hard-scatter (HS) process. At the target anti- k_t jet’s E_T value of 60-100 GeV—the range where the turn-on feature of the efficiency curve activates (discussed later in Fig. 6)—70-90% of primitive jets are matched (discussed later in Fig 5). The reference E_T value of the HS jet is the anti- k_t E_T value of the corresponding offline jet, which is motivated by the assumption that the best trigger performance will be achieved by matching to the offline energy scale as closely as possible. Otherwise, if no match is found, the primitive jet is considered a pileup jet, or “PU jet.”

Machine learning.—The ML is composed of two BDT models, BDT_{ET} and BDT_{HS} , whose outputs are combined at the end. The former performs regression as the “ E_T estimator” and the latter performs classification as a “Hard Scatter tagger.” Both models use the same set of input variables from calorimeters. There are sixteen quantities: η of jet of interest and sets of three E_T values (E_T^{EM} , E_T^{HAD} , E_T^{SUM}) for each of the four rings around the jet shown in Fig. 1 and defined next, where SUM is of the

electromagnetic and hadronic components, as well as the set for the smallest three rings combined as ring_{jet} . Each ring is defined by the sum of 0.1×0.1 tower E_T within the annuli around the η - ϕ center of the jet defined by the following boundaries. The number of 0.1×0.1 towers are given in parentheses with the ring labels: $\Delta R < 0.1$ (4 towers in ring_1), $0.1 \leq \Delta R < 0.2$ (12 towers in ring_2), $0.2 \leq \Delta R < 0.4$ (40 towers in ring_3), and $0.4 \leq \Delta R < 0.6$ (68 towers in ring_4). When we refer to primitive jets, they correspond to $\Delta R < 0.4$ (56 towers in ring_{jet}). Due to their square nature, a tower is included in a given ring if its η - ϕ center is within the annulus definition. Visualization of a 100 GeV jet with rings are shown in Fig. 1.

The ring definitions are guided by the physics process. The most probable E_T distribution for a HS jet is highly energetic with concentration of E_T near the jet center with lower values fading away. In contrast, a PU jet is the sum of stochastic energy deposits so their distributions are not as strongly peaked. Following this logic, the rings are defined so that ring_{jet} is the E_T of the primitive jet; ring_{1-3} are its three concentric decomposition. The two outermost $\text{ring}_{3,4}$ is designed to measure the local pileup level around the jet. On the one hand, we do not expect $\text{ring}_{1,2}$ to be correlated to the ambient E_T density of the due to pileup processes. On the other hand, we expect $\text{ring}_{3,4}$ to be strongly correlated to the ambient E_T density and serve as the input variable to provide *in situ* pileup suppression. To compare the pileup density in each ring, we use the pre-defined pileup density computed as the median of calorimeter tower energies, which we denote as ρ [22]. The median suppresses the upward bias of the mean due to the contribution of jets from the hard scatter process. Figure 2 confirms our expectations by showing the lack of correlation of ring_2 and the strong correlation of ring_4 to ρ . The correlation coefficients for ring_2 and ring_4 are 0.15 (0.13) and 0.52 (0.45), respectively, for EM (HAD).

ML training is done using TMVA [56]. Both BDT_{ET} and BDT_{HS} are each composed of 30 trees with a maximum depth of 8 using adaptive boosting. Half the sample is randomly assigned to training, with the rest assigned

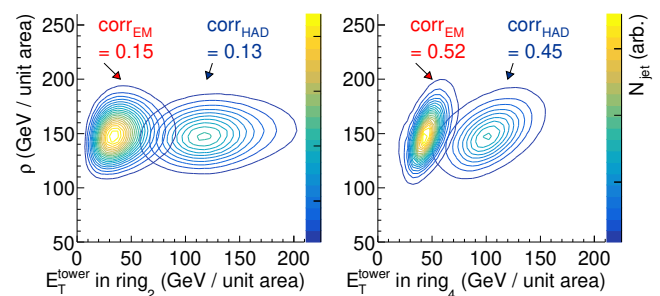


FIG. 2. Correlations between the event E_T density ρ and tower E_T normalized to unit area in η - ϕ for ring_2 (left) and ring_4 (right) defined in the text. In each plot, both the contours of EM and hadronic components are shown separately as well as their correlation coefficients.

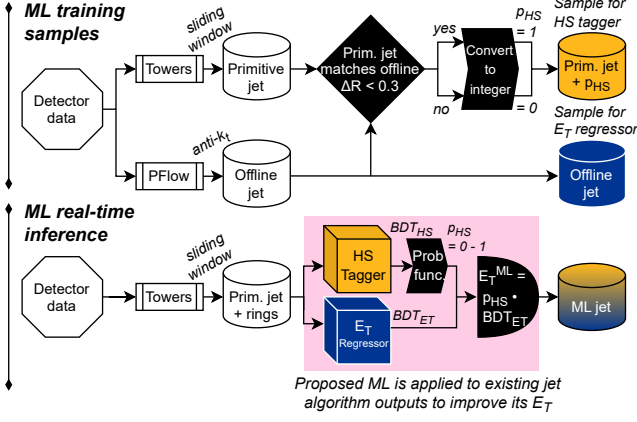


FIG. 3. Flowchart for obtaining the simulated training sample (top) and the real-time inference of incoming data (bottom). The pink box encloses the ML proposed in this paper.

to testing. The workflow to obtain the training sample is shown on the top half of Fig. 3 and described below.

BDT_{ET} is regression trained to estimate the E_T given a primitive jet. It is trained on the sample of offline jets, using only the calorimeter-derived features above as inputs, with the offline E_T calculated by anti- k_t as the target value. As the E_T spectrum of these jets is exponentially decreasing, weighting is applied to effectively flatten the E_T distribution to avoid biasing the BDT in favor of lower E_T . Events are weighted by the inverse of the population of the corresponding bin in the E_T distribution. It is important to note that because the BDT_{ET} is trained on anti- k_t offline jets, it is optimized assuming that any jet under consideration is from hard scatter. We will see that this is a reasonable assumption and that a correction is made for the assumption later in the paper.

We evaluate BDT_{ET} by considering the ratio R of the regressed E_T and the ΔR -matched reference E_T^{offline} , and is compared to the R for primitive jets. These distributions are shown in bins of E_T^{prim} in the left plot of Fig. 4. The R_{prim} distributions are uncalibrated, so they peak at high values of 3.5 in the lowest E_T^{prim} bin, as pileup contribution dominate, while it moves towards unity for higher E_T^{prim} bins as pileup contributions dominate less. In contrast, R_{BDT} ratios hover around unity for all bins showing the effectiveness of *in situ* pileup correction. The modes of the R distribution (\hat{R}) are listed in the left plot and quantifies the amount of pileup in each bin.

The comparison of uncalibrated E_T is made to show the effect of pileup as it does not reflect the performance. To compare the performance, we calibrate each incoming E_T by the \hat{R} derived above for each bin in E_T^{prim} . The resulting distribution centers around unity as shown on the right plot of Fig. 4. The width of the calibrated distributions are listed on the plot along with the percentage gain, $\text{rms}_{\text{BDT}}/\text{rms}_{\text{prim}} - 1$. The E_T ranges of the bins are rescaled by \hat{R}_{prim} to give a range closer to the correspond-

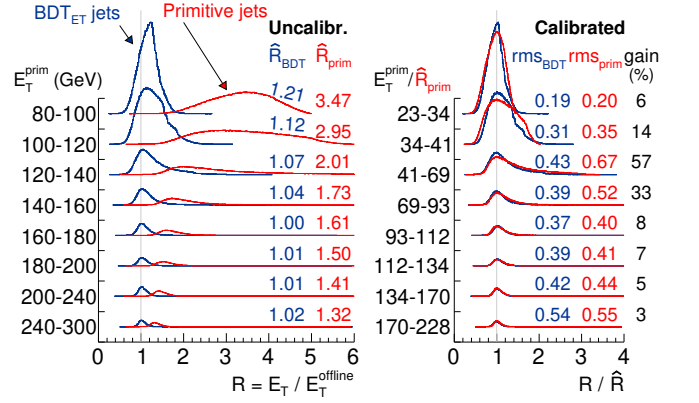


FIG. 4. Performance of BDT_{ET} . Left: Distribution of uncalibrated E_T resolutions in eight slices of E_T^{prim} bins for BDT_{ET} (thick curve) and E_T^{prim} (thin curve). Right: Distribution of calibrated E_T resolutions by dividing by \hat{R} , the mode of R in each slice; the bin range is also rescaled by \hat{R} . After calibration, the rms at unity and the gain with respect to primitive jets are listed.

ing offline values. In the calibrated E_T bin of 69-93 GeV, which is in our target range for HH_{4b} , the rms gain is 33%. If advancements of trigger systems would allow acceptance of lower E_T jets, we note that in the calibrated E_T bin from around 41-69 GeV, the rms gain is doubled at 57%.

Since BDT_{ET} is designed estimate the E_T from primitive jets that originate from the HS process, a correction is made to address the fraction not originating from HS. BDT_{HS} is a classifier trained to categorize primitive jet into HS and PU by utilizing differences in the E_T distribution in each ring. It is trained on the sample of primitive jets using the same set of input features with matched jet given a score of 1 and unmatched jet given a score of 0. The output score of BDT_{HS} is a continuous value between 0 and 1. As expected, the likelihood a primitive jet originates from HS increases with its calorimeter energy, E_T^{prim} . The left plot in Fig. 5 shows that after calibration in the corresponding bin as in the right plot of Fig. 4, primitive jets with calibrated E_T^{prim} in range of interest from 60-100 GeV are likely to originate from HS at 70-90%. The effectiveness of classifying primitive jets as HS using BDT_{HS} is compared to using E_T^{prim} alone is shown by comparing their ROC curves in the right plot of Fig. 5. At 1% (0.01%) acceptance of PU jets, the improvement in efficiency in identifying primitive jets as HS using BDT_{HS} is a factor of 1.2 (3.0) higher than just using primitive jets.

We transform the BDT_{HS} score to a “HS probability” by normalizing to the total number of jets, $p_{\text{HS}} = N_{\text{HS}}/(N_{\text{HS}} + N_{\text{PU}})$, where N_{HS} represents the number of HS events in the bin containing the score in the distribution and likewise for N_{PU} . This probability is used to combine with the output of BDT_{ET} .

Following conventional jet algorithms that use E_T

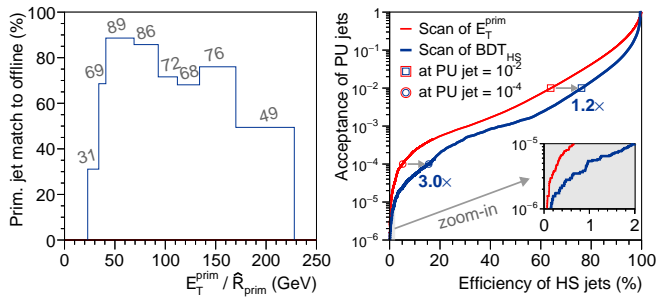


FIG. 5. Performance of BDT_{HS} . Left: Fraction of primitive jets matched to offline jets in bins of the calibrated E_T^{prim} (Fig. 4) using the dijet sample. Right: Acceptance of primitive jets identified as PU vs. efficiency of primitive jets identified as HS with $E_T^{\text{offline}} > 40$ GeV obtained by scans of BDT_{HS} (thick curve) and E_T^{prim} (thin curve) using the HH_{4b} sample.

thresholds to trigger events to keep [57], the final output of the ML is the estimated BDT_{ET} value weighted by the HS probability, p_{HS} . The weighting prioritizes those primitive jets that are likely from HS and to suppress those that are likely from stochastic pileup:

$$E_T^{\text{ML}} = p_{\text{HS}} \cdot \text{BDT}_{\text{ET}}. \quad (1)$$

The workflow for the real-time inference is shown on the bottom row of Fig. 3. The pink box encloses the ML proposed in this paper.

Lastly, the ML must be able to be fit within the constraints of the LHC experiments. Previous work have demonstrated that models with parameters similar to those in our paper can be implemented using percent-level resources with $\mathcal{O}(10)$ ns latency and interval between successive inputs on FPGA [41–44].

Results.—The performance is evaluated using HH_{4b} as the physics process of interest. The impact of HH_{4b} signal acceptance is demonstrated by comparing equal-background-rate efficiency curves constructed using offline jets as reference. The threshold goal for the HL-LHC four-jet trigger at 80% efficiency is set to 90 GeV, consistent with ATLAS in Run 3 [12]. This threshold corresponds to a dijet background acceptance of around 1%, which is used to derive the equal-rate threshold the E_T^{prim} -based trigger. The left plot of Fig. 6 shows the distribution of the E_T^{offline} of the fourth leading jet for HH_{4b} events. The distribution peaks around 50 GeV and rapidly falls at higher values. In particular, the inset shows the region of interest from 80–120 GeV along with the cumulative signal fraction, where we see increases by a factor of 1.5 every 10 GeV.

The right plot of Fig. 6 shows the turn-on curve showing HH_{4b} signal efficiency as a function of E_T^{offline} for the fourth leading jet. The plot shows four curves: two sets, for 5% and 1% dijet acceptance, of a pair of curves for primitive jets and ML jets. We see that the two ML curves becomes fully efficient much quicker than their primitive counterparts. A horizontal line at 80% shows

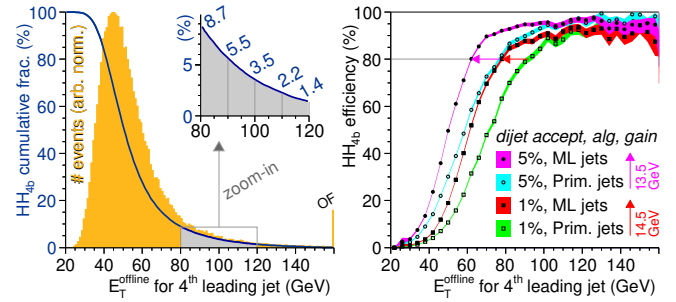


FIG. 6. Performance of ML jets. Left: Distribution of 4th leading jet E_T^{offline} (histogram); cumulative fraction of HH_{4b} above the x -axis threshold (curve). The inset shows the 80–120 GeV region with values. Right: Equal-rate HH_{4b} efficiency vs. 4th leading jet E_T^{offline} for 5% (○) and 1% (□) acceptance of dijet events.

13.5 GeV shift from primitive jets to ML jets for 5% dijet acceptance, and 14.5 GeV shift for 1% dijet acceptance. To compare with existing values, we consider improvement at 80% efficiency. The improvement using ML reduces the threshold from around 90 to 75 GeV there, increasing the signal acceptance by a factor of 2.1. In order to achieve a similar gain without the ML, the background acceptance would need to be increased by a factor of 5. This is demonstrated by the overlap of the “5%, Prim. jets” curve and “1%, ML jets” curve at the horizontal 80% efficiency line. ATLAS projections show that the upper bound on the Higgs self-coupling by lowering the jet threshold improves by a relative 20% [11], although this is without systematic uncertainties so the actual improvement is likely to be lower.

Conclusions.—As limitations on the minimum E_T threshold primarily occur in the L1 trigger, the jet E_T calibration using ML proposed in this paper for the first-level trigger system can lower the fourth leading jet E_T by 10–15 GeV, depending on the starting trigger threshold, for $HH \rightarrow b\bar{b}b\bar{b}$. This, in turn, may help improve the sensitivity of Higgs self-coupling by up to 20%.

ACKNOWLEDGMENTS

We thank Ariel Schwartzman for suggesting ring₄ outside the primitive jet. We thank Steven Schramm pointing out the interplay between classification and regression. We thank Santiago Cané for FPGA estimations for our models. TMH is supported by the US Department of Energy [award no. DE-SC0007914]. BTC is supported by the National Science Foundation [award no. 2209370]. STR was supported by the Emil Sanielevici Scholarship.

-
- [1] O. Aberle, I. Béjar Alonso, O. Brüning, P. Fessia, M. Lamont, L. Rossi, L. Tavian, and M. Zerlauth, eds., *High-Luminosity Large Hadron Collider (HL-LHC): Technical design report*, CERN Yellow Reports: Monographs, 2020, <http://cds.cern.ch/record/2749422>.
 - [2] S. Di Vita, C. Grojean, G. Panico, M. Rimbaut, and T. Vantalón, *A global view on the Higgs self-coupling*, J. High Energy Phys. **09**, 069 (2017).
 - [3] J. Baglio, A. Djouadi, R. Gröber, M. M. Mühlleitner, J. Quevillon, and M. Spira, *The measurement of the Higgs self-coupling at the LHC: theoretical status*, J. High Energy Phys. **04**, 151 (2013).
 - [4] S. Dawson, A. Ismail, and I. Low, *What's in the loop? The anatomy of double Higgs production*, Phys. Rev. D **91**, no.11, 115008 (2015).
 - [5] U. Baur, T. Plehn, and D. L. Rainwater, *Measuring the Higgs Boson Self Coupling at the LHC and Finite Top Mass Matrix Elements*, Phys. Rev. Lett. **89**, 151801 (2002).
 - [6] T. Plehn and M. Rauch, *Quartic Higgs coupling at hadron colliders*, Phys. Rev. D **72**, 053008 (2005).
 - [7] A. Djouadi, W. Kilian, M. Muhlleitner, and P. M. Zerwas, *The Reconstruction of trilinear Higgs couplings*, Proceedings of DESY/ECFA LC Workshop: Physics with a High-Luminosity e^+e^- Linear Collider, DESY 99-123F, 2000, [hep-ph/0001169].
 - [8] ATLAS Collaboration, *Constraining the Higgs boson self-coupling from single- and double-Higgs production with the ATLAS detector using pp collisions at $\sqrt{s} = 13$ TeV*, Phys. Lett. B **843**, 137745 (2023).
 - [9] CMS Collaboration, *Search for nonresonant Higgs boson pair production in the $b\bar{b}b\bar{b}$ final state at $\sqrt{s} = 13$ TeV*, J. High Energy Phys. **04**, 112 (2019).
 - [10] ATLAS Collaboration, *HL-LHC prospects for the measurement of Higgs boson pair production in the $b\bar{b}b\bar{b}$ final state and combination with the $b\bar{b}\gamma\gamma$ and $b\bar{b}\tau^+\tau^-$ final states at the ATLAS experiment*, ATL-PHYS-PUB-2022-053, 2022, <http://cds.cern.ch/record/2841244>.
 - [11] ATLAS Collaboration, *Measurement prospects of the pair production and self-coupling of the Higgs boson with the ATLAS experiment at the HL-LHC*, ATL-PHYS-PUB-2018-053, 2018, <http://cds.cern.ch/record/2652727>.
 - [12] ATLAS Collaboration, *The ATLAS trigger system for LHC Run 3 and trigger performance in 2022*, J. Instrum. **19**, P06029 (2024), see Figure 43.
 - [13] ATLAS Collaboration, *Jet reconstruction and performance using particle flow with the ATLAS Detector*, Eur. Phys. J. C **77**, 466 (2017).
 - [14] CMS Collaboration, *Particle-flow reconstruction and global event description with the CMS detector*, J. Instrum. **12**, P10003 (2017).
 - [15] M. Cacciari, G. P. Salam, and G. Soyez, *The anti- k_t jet clustering algorithm*, J. High Energy Phys. **04**, 063 (2008).
 - [16] P. Berta, M. Spousta, D. W. Miller, and R. Leitner, *Particle-level pileup subtraction for jets and jet shapes*, J. High Energy Phys. **06**, 092 (2014).
 - [17] M. Cacciari, G. P. Salam, and G. Soyez, *SoftKiller, a particle-level pileup removal method*, Eur. Phys. J. C **75**, 59 (2015).
 - [18] ATLAS Collaboration, *Constituent-level pile-up mitigation techniques in ATLAS*, ATLAS-CONF-2017-065, 2017, <http://cds.cern.ch/record/2281055>.
 - [19] P. T. Komiske, E. M. Metodiev, B. Nachman, and M. D. Schwartz, *Pileup Mitigation with Machine Learning (PUMML)*, J. High Energy Phys. **12**, 051 (2017).
 - [20] P. Berta, L. Masetti, D. W. Miller, and M. Spousta, *Pileup and Underlying Event Mitigation with Iterative Constituent Subtraction*, J. High Energy Phys. **08**, 175 (2019).
 - [21] CMS Collaboration, *Pileup mitigation at CMS in 13 TeV data*, J. Instrum. **15**, P09018 (2020).
 - [22] M. Cacciari and G. P. Salam, *Pileup subtraction using jet areas*, Phys. Lett. B **659**, 119 (2008).
 - [23] M. Cacciari, G. P. Salam and G. Soyez, *The catchment area of jets*, J. High Energy Phys. **04**, 005 (2008).
 - [24] CMS Collaboration, *Determination of Jet Energy Calibration and Transverse Momentum Resolution in CMS*, J. Instrum. **6**, 11002 (2011).
 - [25] CMS Collaboration, *Jet energy scale and resolution in the CMS experiment in pp collisions at 8 TeV*, J. Instrum. **12**, P02014 (2017).
 - [26] ATLAS Collaboration, *Jet energy scale and resolution measured in proton-proton collisions at $\sqrt{s} = 13$ TeV with the ATLAS detector*, Eur. Phys. J. C **81**, 689 (2021).
 - [27] ATLAS Collaboration, *New techniques for jet calibration with the ATLAS detector*, Eur. Phys. J. C **83**, 761 (2023).
 - [28] ATLAS Collaboration, *Tagging and suppression of pileup jets with the ATLAS detector*, ATLAS-CONF-2014-018, 2014, <http://cds.cern.ch/record/1700870>.
 - [29] ATLAS Collaboration, *Performance of pile-up mitigation techniques for jets in pp collisions at $\sqrt{s} = 8$ TeV using the ATLAS detector*, Eur. Phys. J. C **76**, 581 (2016).
 - [30] CMS Collaboration, *The CMS trigger system*, J. Instrum. **12**, P01020 (2017).
 - [31] CMS Collaboration, *Performance of the CMS Level-1 trigger in proton-proton collisions at $\sqrt{s} = 13$ TeV*, J. Instrum. **15**, P10017 (2020).
 - [32] R. Achenbach, P. Adragna, V. Andrei, P. Apostologlou, B. Åsman, C. Ay, B. M. Barnett, B. Bauss, M. Bendel, C. Böhm, et al., *The ATLAS level-1 calorimeter trigger*, J. Instrum. **3**, P03001 (2008).
 - [33] CMS Collaboration, *The Phase-2 Upgrade of the CMS Level-1 Trigger*, CERN-LHCC-2020-004, CMS-TDR-021, 2020, <http://cds.cern.ch/record/2714892>.
 - [34] ATLAS Collaboration, *Technical Design Report for the Phase-II Upgrade of the ATLAS TDAQ System*, CERN-LHCC-2017-020 and ATLAS-TDR-029, 2017, <http://cds.cern.ch/record/2285584>.
 - [35] J. Bystricky, D. Calvet, P. Le Du, E. Perez, G. Tarte, J. Ban, H. Evans, J. Mitrevski, J. Parsons, W. Sippach, et al., *Algorithms and architecture for the L1 calorimeter trigger at D0 Run IIb*, IEEE Trans. Nucl. Sci. **51**, 351 (2004).
 - [36] R. Mehdiyev, Z. V. Metreveli, P. Nevski, and D. Salihagic, *Test of Sliding Window Algorithm for Jets Reconstruction in ATLAS Hadronic Calorimeters*, ATL-CAL-99-002, 1999, <http://cds.cern.ch/record/683802>.
 - [37] B. Schlag, *Jet Reconstruction in the ATLAS Level-1 Calorimeter Trigger with Deep Artificial Neural Networks*, Master's thesis, Johannes Gutenberg

- University of Mainz, 2018, CERN-THESIS-2018-388, <http://cds.cern.ch/record/2670301>.
- [38] P. Odagiu, Z. Que, J. Duarte, J. Haller, G. Kasieczka, A. Lobanov, V. Loncar, W. Luk, J. Ngadiuba, M. Pierini, *et al.*, *Ultrafast jet classification at the HL-LHC*, Mach. Learn. Sci. Tech. **5**, 035017 (2024).
 - [39] J. Duarte, S. Han, P. Harris, S. Jindariani, E. Kreinar, B. Kreis, J. Ngadiuba, M. Pierini, R. Rivera, N. Tran, *et al.*, *Fast inference of deep neural networks in FPGAs for particle physics*, J. Instrum. **13**, P07027 (2018).
 - [40] T. Aarrestad, V. Loncar, N. Ghielmetti, M. Pierini, S. Summers, J. Ngadiuba, C. Petersson, H. Linander, Y. Iiyama, G. Di Guglielmo, *et al.*, *Fast convolutional neural networks on FPGAs with hls4ml*, Mach. Learn. Sci. Tech. **2**, 045015 (2021).
 - [41] T. M. Hong, B. Carlson, B. Eubanks, S. Racz, S. Roche, J. Stelzer, and D. Stumpp, *Nanosecond machine learning event classification with boosted decision trees in FPGA for high energy physics*, J. Instrum. **16**, P08016 (2021).
 - [42] B. Carlson, Q. Bayer, T. M. Hong, and S. Roche, *Nanosecond machine learning regression with deep boosted decision trees in FPGA for high energy physics*, J. Instrum. **17**, P09039 (2022).
 - [43] P. Serhiayenka, S. Roche, B. Carlson, and T. M. Hong, *Nanosecond hardware regression trees in FPGA at the LHC*, Nucl. Instrum. Method A **1072**, 170209 (2025).
 - [44] S. Summers, G. Di Guglielmo, J. Duarte, P. Harris, D. Hoang, S. Jindariani, E. Kreinar, V. Loncar, J. Ngadiuba, M. Pierini, *et al.*, *Fast inference of Boosted Decision Trees in FPGAs for particle physics*, J. Instrum. **15**, P05026 (2020).
 - [45] S. T. Roche, B. T. Carlson, and T. M. Hong, *fwXmachina example: Jet energy resolution*, Mendeley Data, 2025, doi:10.17632/v9z86dp9mv.1.
 - [46] ATLAS Collaboration, *Simulation of Pile-up in the ATLAS Experiment*, J. Phys.: Conf. Ser. **513**, 022024 (2014).
 - [47] G. Apollinari, O. Brüning, T. Nakamoto, and L. Rossi, *High Luminosity Large Hadron Collider HL-LHC*, CERN Yellow Rep. **5**, 1–19 (2015).
 - [48] Longer term LHC schedule, “Update September 2024,” <https://lhc-commissioning.web.cern.ch/schedule/LHC-long-term.htm>, accessed July 14, 2025.
 - [49] J. Alwall, M. Herquet, F. Maltoni, O. Mattelaer, and T. Stelzer, *MadGraph 5: Going Beyond*, J. High Energy Phys. **06**, 128 (2011).
 - [50] T. Sjöstrand *et al.*, *An introduction to PYTHIA 8.2*, Comput. Phys. Commun. **191**, 159–177 (2015).
 - [51] DELPHES 3 Collaboration, *DELPHES 3, A modular framework for fast simulation of a generic collider experiment*, J. High Energy Phys. **02**, 057 (2014).
 - [52] ATLAS Collaboration, *The ATLAS Experiment at the CERN Large Hadron Collider*, J. Instrum. **3**, S08003 (2008).
 - [53] ATLAS Collaboration, *Technical Design Report for the Phase-I Upgrade of the ATLAS TDAQ System*, CERN-LHCC-2013-018 and ATLAS-TDR-023, 2013, <http://cds.cern.ch/record/1602235>.
 - [54] M. Cacciari, G. P. Salam, and G. Soyez, *FastJet User Manual*, Eur. Phys. J. C **72**, 1896 (2012).
 - [55] Algorithm in four steps: generate seeds, require local maxima, apply threshold, and find jet centers. (1) Each 0.1×0.1 tower generates a 0.3×0.3 square “seed” from the neighboring towers in each direction, whose sum E_T is the E_T^{seed} . (2) Each seed is compared to the seed E_T of the other 24 seeds centered within a 0.5×0.5 square around it. Only keep seeds that has the greatest E_T^{seed} among its neighbors. (3) Discard seeds with $E_T^{\text{seed}} < 20$ GeV. (4) The remaining seeds are the centers of the primitive jets.
 - [56] A. Hoecker, P. Speckmayer, J. Stelzer, J. Therhaag, E. von Toerne, H. Voss, M. Backes, T. Carli, O. Cohen, A. Christov, *et al.*, *TMVA – Toolkit for Multivariate Data Analysis*, CERN-OPEN-2007-007, 2007, [physics/0703039].
 - [57] ATLAS Collaboration, *Trigger menu in 2018*, ATL-DAQ-PUB-2019-001, 2019, <http://cds.cern.ch/record/2693402>.